KSCE Journal of Civil Engineering (2012) 16(4):465-477
DOI 10.1007/s12205-012-1256-7

Coastal and Harbor Engineering

www.springer.com/12205

Analysis of the 3D Zone of Flow Establishment from a Ship's Propeller

Wei-Haur Lam*, Gerard Hamill, Desmond Robinson***, Srinivasan Raghunathan****, and Yongchen Song*******

Received June 26, 2010/Revised 1st: May 6, 2011, 2nd: June 27, 2011/Accepted August 24, 2011

Abstract

In the present study an experimental investigation of the time-averaged velocity and turbulence intensity distributions from a ship's propeller, in "bollard pull" condition (zero speed of advance), is reported. Previous studies have focused mainly on the velocity profile of not a rotating ship propeller but a plain jet. The velocity profile of a propeller is investigated experimentally in this study. The velocity measurements were performed in laboratory by using a Laser Doppler Anemometry (LDA). The measurements demonstrated two-peaked ridges velocity profile with a low velocity core at the centre within the near wake. The two-peaked ridges combined to be one-peaked ridge at 3.68 diameters downstream indicating the end of the zone of flow establishment. The study provides useful information from a rotating ship's propeller rather than a simplified plain jet to researchers investigating flow velocity generated from a propeller and probably resulting local scouring.

Keywords: *ship's propeller jet, Laser Doppler Anemometry (LDA), zone of flow, establishment*

1. Introduction

The investigations of the fluid flows within the ship's propeller wash which can lead to seabed scouring are of particular interest for the design of marine structures. In Whitehouse (1998)'s book "Scour at Marine Structures", the potential damage made by the propeller wash is highlighted. The action of the propeller wash to the seabed scouring is also described in Sumer and Fredsøe (2002) book "The Mechanics of Scour in the Marine Environment" and Gaythwaite (2004)'s book "Design of Marine Facilities for the Berthing, Mooring, and Repair of Vessels". The jet impingement of a ro-ro ship to the seabed is illustrated in Fig. 1.

An unconfined propeller jet is preliminary investigated in order to determine the propeller induced seabed scouring. The influences of the rudder (Ryan, 2002; Hamill *et al*., 2009), hull and the berth geometry to the velocity within the wash will normally be included after the unconfined propeller jet being established. The impingement velocities are therefore used to determine the erosion extent and erosion rate within the seabed (Bergh and Cederwall, 1981; Fuehrer and Römisch, 1987; Dargahi, 2003; van Blaaderen, 2006). The influence of the bed material, which resists jet impingement, will be considered in order to propose an effective remedial action (Prosser, 1986). The problem of the ship's induced scour was also investigated by using a simplified round jet, which has been documented by Yeh *et al*. (2009) and Yülsel *et al*. (2005). The general problem of the propeller wash is presented in Fig. 2.

Albertson *et al*. (1950) used a plain water jet to investigate the velocity field within the jet based on axial momentum theory. The flow pattern of a plain water jet can be divided into two zones, the zone of flow establishment and the zone of established flow by observing the changes of the velocity field. Albertson *et al*. (1950)'s works has been the basis of all subsequent work with propeller jets. Several researchers have carried out investigations using physical model to determine the velocity magnitudes within a ship's propeller jet (Blaauw and van de Kaa, 1978; Berger *et al*., 1981; Verhey, 1983; Hamill, 1987). These researchers investigated the velocity field within a ship propeller jet using an actual propeller to compensate the flaw inherited from the investigations of a plain water jet. Hamill (1987) measured the velocity field induced by a propeller model in laboratory using Pitot tube and found the differences between a ship's propeller jet and a plain water jet (Figs. 3 and 4).

Hamill *et al*. (2004), van Blaaderen (2006) and Yülsel *et al*. (2005) investigated the velocity field with different main focuses. Hamill (1987) investigated the velocity field within the jet from a

*Associate Professor, Dept. of Civil Engineering, University of Malaya, 50603 Kuala Lumpur, Malaysia (Corresponding Author, E-mail: wlam@um.edu.my)
**Senior Lecturer, Queen's University Belfast, Northern Ireland BT9 5AG, UK (E-mail: g.a.hamill@qub.ac.uk)
***Senior Lecturer, Queen's University Belfast, Northern Ireland BT9 5AG, UK (E-mail: des.robinson@qub.ac.uk)
****Emeritus Professor, Queen's University Belfast, Northern Ireland BT9 5AH, UK (E-mail: s.raghunathan@qub.ac.uk)
*****Professor, Key Laboratory of Ocean Energy Utilization and Energy Conservation of Ministry of Education, Dalian University of Technology, Dalian, Liaoning 116024, China (E-mail: powere@dlut.edu.cn)

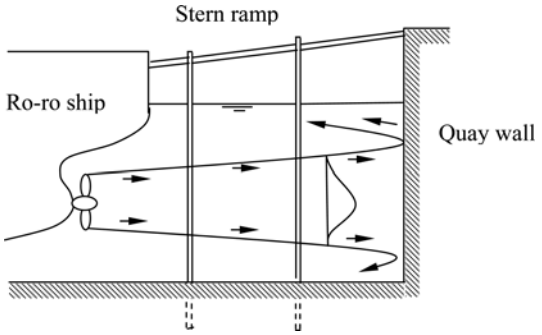

Fig. 1. Jet Impingement in the Case of Ro-ro Ship with Stern Ramp, Sumer and Fredsøe (2002)

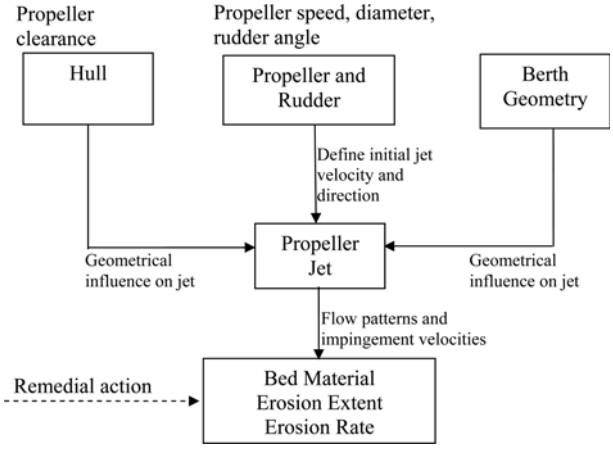

Fig. 2. Parameters of the Seabed Scouring (Prosser, 1986)

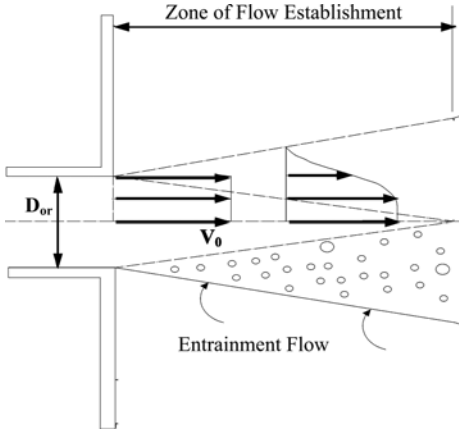

Fig. 3. Schematised Representation of a Diffusing Jet from an Orifice, Albertson *et al*. (1950)

rear ship's propeller, whereas van Blaaderen (2006) believed that the bow-thruster is the main cause to the propeller jet induced damage and therefore the velocity field produced by a bow-thruster is of his particular interest. Yülsel *et al*. (2005) used a rotating round water jet to model a ship's propeller jet for his seabed damage research. Lam *et al*. (2012, 2011a, 2011b, 2011c, 2010) proposed the investigation of the problem by using a ship's propeller jet instead of the round water jet. Current investigation may be useful for the researches of discharging water jet

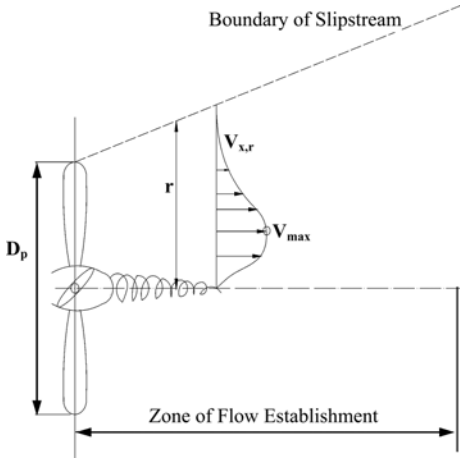

Fig. 4. Schematic Representation of Propeller Jet, Hamill (1987)

in wastewater system (Kwon and Seo, 2005; Seo *et al*., 2004; Kim and Seo, 2004; Kang *et al*., 1999), which the velocity profile and mixing characteristics of the plain jet are the particular focus instead of a rotating ship's propeller jet in this investigation.

In this study, a Laser Doppler Anemometry (LDA) measurement system was adopted to measure the time-averaged velocity and turbulence intensity within the zone of flow establishment from a rear ship's propeller. LDA is a non-intrusive optical measurement technique which could be used to measure the time-averaged velocity and turbulence intensity simultaneously at a point in a flow. The non-intrusive method meant the system would not influence the original flow as happened with the Pitot tube system. Previous studies have focused mainly on the velocity profile of not a rotating ship propeller but a plain jet. Current investigation provides useful data to researchers investigating flow velocity generated from a propeller and probably resulting local scouring.

2. Methodology

An experimental programme using a small propeller was carried out in laboratory. Laser Doppler Anemometry (LDA) was used to simultaneously measure the three main components of velocity, along with the turbulence intensity, within the wash produced by the propeller while it acted under bollard pull conditions. The measurements were validated by comparing the repeatability between the 2D and 3D LDA measurements.

2.1 Experimental Set-up

The experimental apparatus was set up in the hydraulics laboratory in Queen's University Belfast. A water tank which was large enough to allow the unhindered expansion and diffusion of the propeller jet was used in a series of experiments. The purpose built test tank was 7.5 m×4.4 m in plan by 1.0 m deep (Fig. 5). The tank was filled to a height of 880 mm before the measurement started. The submerged propeller was located at almost mid-depth in the tank (440 mm). Stewart (1992) reported that the effect of the tank bottom and water boundaries was not found to influence

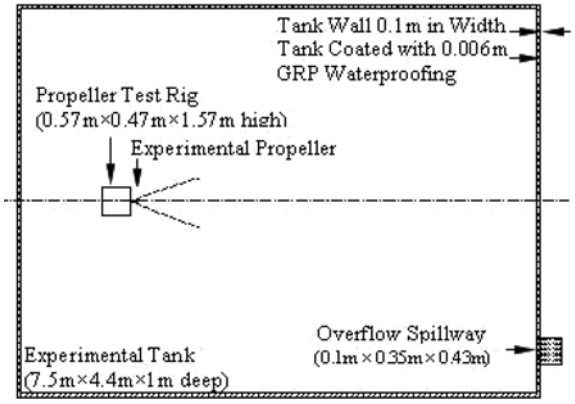

Fig. 5. Schematic Representation of Experimental Tank

the free expansion of the unconfined jet under investigation.

The present study was undertaken using a small propeller at "bollard pull" condition (zero advance speed). The propeller was fitted to a stainless steel shaft on a stationary rig to allow the rotation at the zero advance speeds. A central nut, 20 mm in diameter, was used to lock the propeller to the shaft. The propeller rig was located along the centreline of the water tank about 1.5 m from the rear. The circulation effect of water within the tank has been shown to be insignificant to the jet expansion. A small propeller was used for the experimental measurement due to the limitation of laboratory space. The propeller characteristics are shown in Table 1. The definition of the propeller terms can be found in (Carlton, 1994; EN-ISO-3715-1, 2004; Gerr, 2001).

2.2 Scaling of Experimental Model

Verhey (1983) suggested that the scaling effects due to viscosity were negligible if the Reynolds number of the propeller and the Reynolds number of the flow were greater than 7×10^4 and 3×10^3 respectively. Verhey (1983) calculated the Reynolds number of the propeller (Re_{prop}) and the Reynolds number of the flow (Re_{flow}) using:

$$Re_{flow} = \frac{V_o D_p}{\nu} \quad (1)$$

$$Re_{prop} = \frac{nD_p L_m}{\nu} \quad (2)$$

where the V_o is the efflux velocity of the propeller jet, D_p is the propeller diameter, ν is the kinematic viscosity of the fluid (kinematic viscosity of water at 15ºC is 1.141×10^6 m^2/s), n is the number of revolutions per second and L_m is a length term dependant on the blade area ratio (β), number of blades of the propeller (N), diameter of hub (D_h) and propeller diameter (D_p). The L_m term defined by Blaauw and van de Kaa (1978) is:

$$L_m = \beta \cdot D_p \cdot \pi\left(2N\left(1-\frac{D_h}{D_p}\right)\right)^{-1} \quad (3)$$

The efflux velocity (V_o) is the maximum velocity at the face of the propeller, Fuehrer and Rmisch (1977), which is:

$$V_0 = 1.59 n D_p \sqrt{C_t} \quad (4)$$

where n is the rotational speed of the propeller in revolution per second (rps), D_p is the propeller diameter in metres and C_t is the thrust coefficient of the propeller.

According to a survey of British ports and harbours by Qurrain (1994), the typical size and speed of rotation of a propeller which may cause seabed scouring, range from 1.5 to 3 m in diameter with operating speeds of approximately 200 rpm. In this study a typical ship's propeller having a diameter of 2.5 m and a thrust coefficient $C_t = 0.35$ operating at a rotational speed of 200 rpm was used as a prototype for the 76 mm diameter propeller. The initial efflux equation (V_o) calculated from Eq. (4) is 7.84 m/s. Using the following scaling relationship suggested by Stewart (1992) the initial efflux velocity may also be calculated:

$$V_{o(\mathrm{mod}\,el)} = V_{o(prototype)}\sqrt{\frac{D_{p(\mathrm{mod}\,el)}}{D_{p(prototype)}}} \quad (5)$$

According to Froudian scaling law, the efflux velocity for a propeller 76 mm that would correspond to these typical operating conditions would be 1.37 m/s. Back calculating to get an operational rotation speed yielded a value of 1075 rpm. It was therefore decided to carrying out this investigation at a rotational speed of 1000 rpm and the corresponding Reynolds number of the propeller (Re_{prop}) and the Reynolds number of the flow (Re_{flow}), calculated using Eqs. (1) and (2), are shown in Table 2.

The Reynolds numbers of the proposed speeds of rotation were compared to Verhey (1983)'s suggestion to identify the influence of the scale effects due to viscosity. The Reynolds numbers due to the flow for the propeller exceeded Verhey (1983)'s suggestion. The Reynolds numbers due to the propeller were slightly lower than 7×10^4, however Blaauw and van de Kaa (1978) and Verhey (1983) proposed that these scale effects were insignificant. The Reynolds number for the jet is greater than 3×10^3 satisfying the criteria for Froudian scaling.

2.3 Measurement Grid

Hamill (1987) concluded that the propeller jet was axisym-

Table 1. Propeller Characteristics

	Propeller-76
Propeller diameter, D_p	76 mm
Hub diameter, D_h	14.92 mm
Blade number, N	3
Rake angle, è	0º
Pitch Ratio (P')	1
Blade area ratio, β	0.473
Thrust coefficient, C_t	0.4

Table 2. Reynolds Number of the Propeller (Re_{prop}) and Reynolds Number of the Flow (Re_{flow})

Propeller	Speeds of rotation	Re_{flow}	Re_{prop}
Propeller-76 (C_t=0.4, D_h=15.2 mm, D_p=76 mm, β=0.473, N=3)	1000rpm	8.5×10^4	2.6×10^4

metric about the axis of rotation. The measurement using a two-dimensional plane about the axis of rotation could represent the entire velocity field. The velocity field was therefore measured using a two-dimensional grid about the axis of rotation. Vertical and horizontal planes were set in order to measure the three components of velocity. The vertical plane was able to measure the axial and the radial components of velocity. The horizontal plane was able to measure the axial and tangential component of velocity.

In the current tests, the measurement of the propeller jet was taken up to $x/D_p = 3.68$ that covered the entire zone of flow establishment. A finer measurement grid was employed to measure the velocity field near to the propeller face and these positions of measurement point are shown in Fig. 6. A 5 mm×20 mm grid was chosen to measure the velocity field from the propeller face up to 160 mm (x/D_p=2.11) downstream. For the region within 160 mm to 280 mm (x/D_p=2.11 to x/D_p=3.68), a 10 mm× 20 mm grid was used to acquire the velocity field.

2.4 Laser Doppler Anemometry

A Dantec Fiber-flow™ optical 5 beam probe was employed to measure the simultaneous values of the axial, tangential and radial components of velocity within the propeller jet, Dantec (2003). The laser beams were initially generated by a water-cooled Stabilite 2017 5W Argon-Ion laser generator manufactured by Spectra Physics. The shifted and unshifted laser beams were focused into fibre optics cables used to carry the laser beams to the transmitting/receiving optical probe (model no. 5402-01). The focus length of the probe was 310 mm which meant that the measurement volume was at a sufficient distance from the probe body to be unaffected by its presence.

2.4.1 Flow Seeding

A seeding tank was built to continually supply the seeding particles to the flow. The impeller on the top stirred the seeding to make it homogeneous. Then the seeding particles were released upstream of the propeller during the measurement. The seeding was passivated aluminium particles (E3064AR) with a 36 μm particle size and density 1.46 g/cm^3. The use of the seeding tank provided a high concentration of seeding to the jet. During measurement process the average recorded burst count due to seeding was 6898 particles with a maximum 14939 particles and a minimum 3982 particles during the 50 second measurement window. Fig. 7 shows the axial velocity output at maximum velocity point on the initial efflux plane, with maximum total burst count of 14939 events.

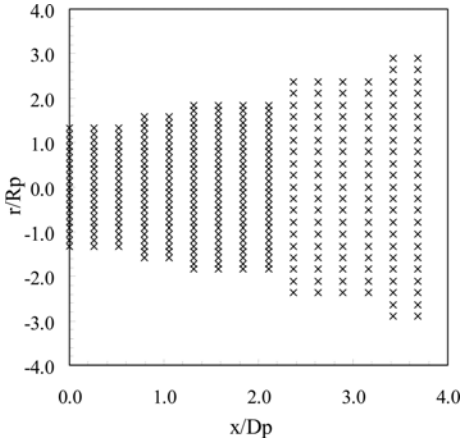

Fig. 6. Positions of Measurement Point within Grid

2.5 Experimental Procedure

The measurement volume was initially aligned at the 'home' position located 10mm downstream at the centreline of propeller hub. The Cartesian coordinate at 'home' position was recognized as (0, 0, 0) in X, Y, Z direction. The measurement grid was therefore generated using BSA flow software to enable the traverse system travelling to each measurement points automatically. For the experiment with 50 seconds acquisition time at each point, the total acquisition time could be estimated by summation of acquisition time for each point plus 5 seconds transition period to allow the traverse system travelling to the following point. The seeding particles were filled into the seeding tanks to provide continual seeding particles during data acquisition. During the acquisition, the continual supply of seeding, the recorded data rate and the burst signal due to the scattered light were monitored to ensure the high quality of data being produced. For each measurement point, 50 seconds was used to acquire sufficient data to minimise the sampling bias. The data rate per second and pattern of burst signal was monitored during the acquisition process. The average data rate for experiment of 76 mm diameter propeller was 164 particles per second.

2.6 Source of Errors

The sampling bias for a 95% confidence limit of time-averaged velocity, turbulence intensity and Reynolds stresses are computed automatically by the LDA system during the data acquisition based on the following equation, Dantec (2003):

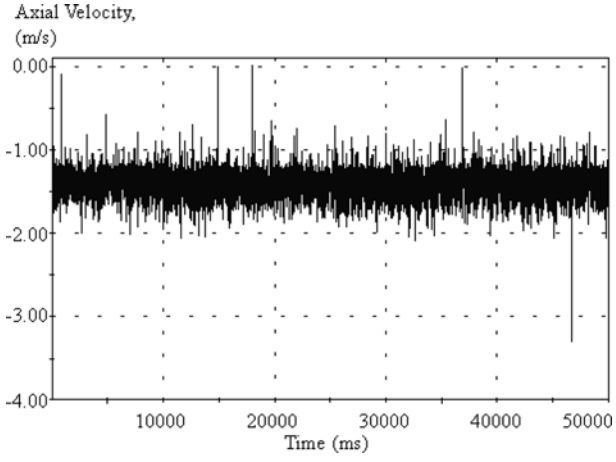

Fig. 7. Axial Velocity Output at Maximum Velocity Point at Initial Efflux Plane with Maximum Total Burst Count 14939 for 50 Seconds

$$U_{mean} = 1.96 \times \sqrt{\frac{\overline{u'^2}}{N_s}} \quad (6)$$

$$U_{RMS} = 1.96 \times \sqrt{\frac{\overline{u'^2}}{2N_s}} \quad (7)$$

where $\sqrt{\overline{u'^2}}$ is the Root Mean Square (RMS) of the velocity component and N_s is the size of sample. For reliable results the equations above requires a large number of samples, N_s, at least 30-50 samples and preferably more, Dantec (2003). In this experiment, the range of sample N_s was in between 3056 to 14939, with an average 6898 samples at each measurement point. The sampling bias is inverse proportional to the sample N_s.

The use of large sample N_s could reduce the sampling bias of the mean velocity and RMS. Based on the calculated data from the LDA system, the sampling bias for 95% confidence limits at each measurement points were close to zero. The sampling bias at the position where the maximum velocity occurred (efflux velocity) is only 0.01 m/s.

2.7 Repeatability

Figure 8 shows the comparison of the axial, tangential and radial components of velocity acquired from 2D and 3D LDA measurement systems to investigate the repeatability of the experimental results. The figure shows high repeatability of the flow pattern reported by the earlier researchers including Hamill (1987), Stewart (1992) and McGarvey (1996). The three researchers reported that the axial velocity was the most dominant velocity component in the jet when compared to the magnitude of the tangential and radial components of velocity. At lateral sections close to the propeller, the axial distribution increased in magnitude from the rotation axis to a maximum before decaying towards the blade tips. McGarvey (1996) reported the radial component has a low velocity magnitude along the rotation axis. These phenomena were observed in both the 2D and 3D LDA measurements.

The 2D measurement system has four laser beams forming two measurement volumes. The 2D system was therefore able to measure two velocity components simultaneously. The axial and tangential components of velocity were acquired when measuring two components at horizontal plane, whereas the axial and radial components of velocity were acquired when measuring two components at vertical plane. The 3D measurement system consisted of five laser beams forming three measurement volumes and each measurement volume corresponded to one velocity component. The axial, tangential and radial components of velocity were therefore able to be measured simultaneously using a 3D system. Fig. 8 shows the comparison of the velocity components acquired from 2D and 3D LDA measurement systems at the initial efflux plane. The axial, tangential and radial components of velocity of two measurement systems are in close agreement.

3. Results and Discussions

Plots of the time-averaged axial, tangential and radial components of velocity and turbulence intensity are shown in Figs. 9-14. The lateral section from the rotation axis to the jet boundary was plotted instead of a full section across the propeller jet due to the axisymmetrical characteristic of the jet. These velocities have been nondimensionlized by the predicted maximum axial velocity at the efflux plane, which was 1.365 m/s for LDA.

3.1 Axial Component of Velocity

The axial component of velocity is the main contributor to the total velocity magnitude. Earlier researchers were solely interested in the axial velocity field within the ship's propeller jet, due to the large contribution made by the axial velocity to seabed scouring. The axial component of velocity shows two velocity peaks at the zone of flow establishment from 0 mm (x/D_p=0) to 280 mm (x/D_p=3.68), with a low velocity core at the centre (Fig. 9). Further downstream of the propeller jet, the two velocity peaks combine into one velocity peak. The flow structure is similar to that reported by Hamill (1987), Stewart (1992), Hashmi (1993), McGarvey (1996) and Brewster (1997). The lateral distribution of the axial component of velocity is wavy, and is not the perfect Gaussian distribution assumed by Albertson *et al*.

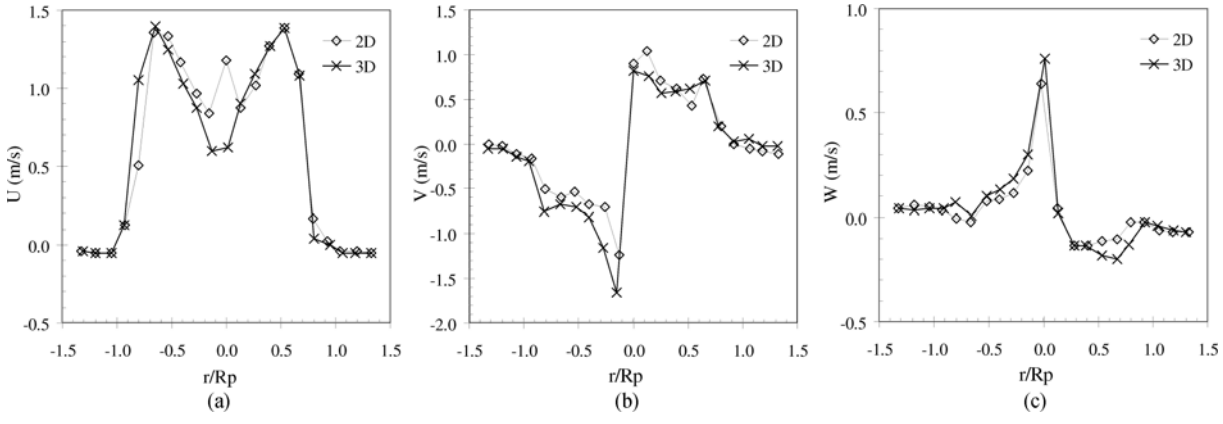

Fig. 8. Comparison of the 2D and 3D LDA Measurement Systems at Efflux Plane: (a) Axial Component of Velocity, (b) Tangential Component of Velocity, (c) Radial Component of Velocity

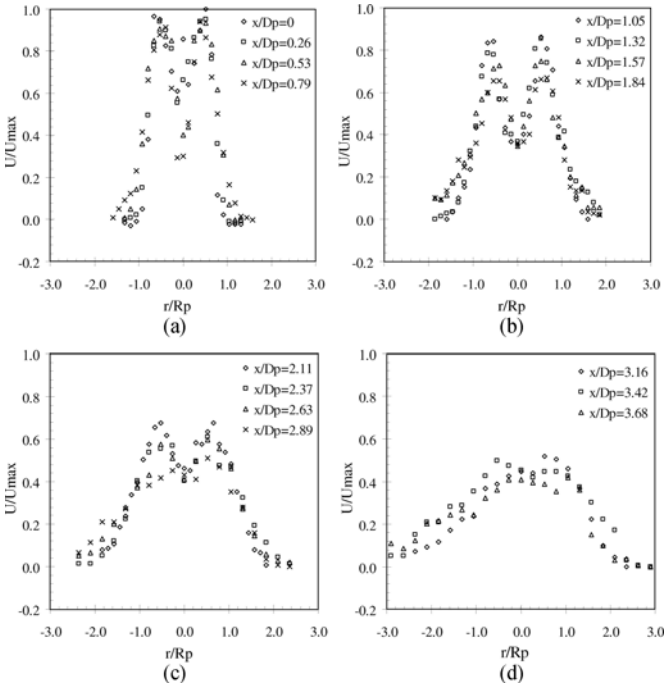

Fig. 9. Dimensionless Axial Velocity Distribution within Zone of Flow Establishment: (a) x/D_p=0, 0.26, 0.53, 0.79, (b) x/D_p=1.05, 1.32, 1.57, 1.84, (c) x/D_p=2.11, 2.37, 2.63, 2.89, (d) x/D_p=3.16, 3.42, 3.68

(1950). The jet boundary is also not a perfectly linear line as assumed by Albertson *et al*. (1950), but the jet boundary is also wavy due to the fluid mixing.

3.1.1 Axisymetric about Rotation Axis

All earlier researchers (Blaauw and van de Kaa, 1978; Berger *et al*., 1981; Verhey, 1983; Hamill, 1987; Stewart, 1992; Hashmi, 1993; McGarvey, 1996; Brewster, 1997) agreed that a propeller jet is axisymetric about the rotation axis from their empirical analysis. The level of symmetry has not been reported by the earlier researchers yet. Fig. 9 shows the lateral sections of the 76mm diameter propeller along the rotation axis within zone of flow establishment. The propeller jet in the zone of flow establishment was reasonably axisymetric about the rotation axis. From the efflux plane (x/D_p=0) up to x/D_p=2.63 downstream, the lateral sections show strong axisymetrical peak velocity profiles at both sides about the rotation axis. In this region, the departure from symmetry are relatively small compared to the sections after x/D_p=2.63 downstream.

From x/D_p=2.89 to x/D_p=3.42 downstream, two-peaked profiles become less axisymetric and sway to the left and right. An analysis is undertaken in order to determine the axisymetrical variation using a simple arithmetic calculation. The variation is calculated based on:

$$\text{variation } (\%) = \left|\frac{V_{left} - V_{right}}{V_{ref}}\right| \times 100\% \quad (8)$$

where V_{ref} is the bigger value of either V_{left} or V_{right}.

Table 3 shows the axisymetrical variation from Equation 8 at various lateral sections from propeller face up to x/D_p=3.68 based on a half-width analysis. Half-width is a lateral extension to a position is half of the peak velocity value ($0.5V_{max}$). Half-width is normally used to avoid the distorted flow pattern at the edge of a jet. The maximum axisymetrical variation at efflux plane (x/D_p=0) is 19%. The maximum axisymetrical variation, which is 48%, occurs at x/D_p=3.16. The axisymetrical variation outside the half-width region may be larger. However, the comparison of the values close to the jet edges is difficult due to the

Table 3. Axisymetrical Variation at Various Lateral Sections (r/R_p, R_p=propeller radius) from Propeller Face up to x/D_p=3.68 Downstream (D_p=propeller diameter)

x/D_p	0.00	0.26	0.53	0.79	1.05	1.32	1.58	1.84	2.11	2.37	2.63	2.89	3.16	3.42	3.68
2.11															
1.97															
1.84															
1.71															
1.58														7%	38%
1.45															
1.32										31%	3%	3%	39%	23%	26%
1.18															
1.05						22%	10%	5%	18%	14%	19%	8%	48%	17%	41%
0.92				24%	2%	11%	23%	25%	7%						
0.79			14%	24%	3%	13%	15%	25%	0%	12%	22%	18%	27%	5%	8%
0.66	19%	8%	2%	16%	3%	6%	10%	11%	3%						
0.53	5%	1%	3%	2%	3%	9%	5%	1%	6%	9%	4%	18%	25%	10%	7%
0.39	8%	5%	3%	3%	13%	29%	0%	7%	7%						
0.26	5%	6%	0%	16%	12%	34%	11%	29%	9%	13%	3%	10%	3%	12%	4%
0.13	4%	26%	24%	36%	9%	19%	8%	24%	5%						
0.00															
Max.	19%	26%	24%	36%	13%	34%	23%	29%	18%	31%	22%	18%	48%	23%	41%

wavy flow pattern and low velocity magnitude. High axisymetrical variation also occurs close to the rotation axis especially in sections x/D_p=0.26, x/D_p=0.53 and x/D_p=0.79.

Albertson *et al*. (1950) assumed 'the diffusion process is dynamically similar under all conditions'. Blaauw and van de Kaa (1978) interpreted the dynamically similarity as requiring all the forces at points with the same radial distance from the rotation axis and same section to be the same, and therefore a propeller jet is axisymetric under this condition. In reality, a ship's propeller jet is only approximately axisymetric. The variation between the velocity values of two sides about the rotation axis is up to 48% within the zone of flow establishment, based on the half-width analysis.

3.1.2 Efflux Velocity

The efflux velocity of a jet is defined as the maximum velocity generated at the propeller plane, Stewart (1992). The derivation of the axial momentum theory yields Eq. (4). This equation has been adopted by the majority of researchers to predict the efflux velocity. Hamill (1987), Stewart (1992) and Hashmi (1993) refined this theoretical equation through experimental investigation. The current investigation shows the measured values of efflux velocity are 1.39 m/s and 1.34 m/s with an average 1.365 m/s. The comparisons of the measured efflux velocity with the value proposed by earlier works are shown in Table 4.

Current measurements validated the equation of axial momentum theory and also those proposed by Hamill (1987), Stewart (1992) and Hashmi (1993) with variation 6.7%, 21.9%, 9.9% and 10.4% respectively. The consideration of geometrical characteristics of a propeller by Stewart (1992) and Hashmi (1993) seemed to reduce the deviation from the measured value.

The experimental measurements showed the positions of maximum velocity are at 20 mm and 25 mm radial distance from the rotation axis with an average of 22.5 mm. Berger *et al*. (1981) proposed the equation $R_{mo} = 0.67(R_pR_h)$ to predict the location of maximum axial velocity, from the rotation axis, at the efflux plane. When R_p is 38mm and R_h is 7.46 mm in this study, the position of the efflux velocity is therefore 20.46 mm radial distance from the rotation axis based on Berger *et al*. (1981)'s equation. The variation between the current measurement and Berger *et al*. (1981)'s equation is 10%. Current measurement also supports the argument of Berger *et al*. (1981), Prosser (1986), Hamill (1987), Stewart (1992) and McGarvey (1996) that the position of the maximum velocity at the efflux plane is not located at the rotation axis, as it would be for a plain water jet.

Blaauw and van de Kaa (1978), Verhey (1983) and Robakiewicz (1987) suggested contraction happens at the efflux plane based on the equation derived from continuity equation (contraction should happen at a radial distance of 26.9 mm from the rotation axis for the 76 mm diameter propeller). Current measurement shows the axial velocity at a radial distance of 26.9 mm is about 0.16 m/s. There is the possibility that the contraction occurs but could be bigger than $0.707D_p$ as suggested by continuity equation.

3.1.3 Length of Zone of Flow Establishment

The zone of the flow establishment shows two peak values across the section with a lower velocity at the rotation axis, Hamill (1987). The length of the zone of the flow establishment is defined by the position where the two peaks combine into one peak position at the rotation axis, Stewart (1992).

Figure 9 shows that two velocity peaks occurs at various sections along the rotation axis. The two velocity peaks have nearly combined by x/D_p=2.63 downstream and have eventually combined at x/D_p=3.68 (Fig. 9). Table 5 shows the variation between the peak and central core velocities at various sections along the rotation axis. The zone of flow establishment ends when two velocity peaks combine into one peak after several propeller diameters downstream. The measurements founds the variations between magnitudes of two velocity peaks from x/D_p=0.53 up to x/D_p=3.42 are in a range of 9% and 67%. At section x/D_p=3.42, two velocity peaks occur at the section with the same velocity magnitude. Two velocity peaks combines into one peak at x/D_p=3.68 and the length of zone of flow establishment is therefore taken as x/D_p=3.68.

Table 4. Comparison of Efflux Velocity between Current LDA Measurements and Previous Works

Source	Equation	Efflux velocity	Variation
Measured value	-	1.365 m/s	-
Axial momentum theory	$V_0 = 1.59nD_p\sqrt{C_t}$ n=16.67 revolution/s D_p=0.076m C_t=0.4	1.274 m/s	6.7%
Hamill (1987)	$V_o = 1.33nD_p\sqrt{C_t}$	1.066 m/s	21.9%
Stewart (1992)	$V_o = \varsigma nD_p\sqrt{C_t}$ $\varsigma = D_p^{-0.0686}P'^{1.519}\beta^{-0.323}$ P'=1.0 β=0.47	1.230 m/s	9.9%
Hashmi (1993)	$V_o = E_o nD_p\sqrt{C_t}$ $E_o = \left(\frac{D_p}{D_h}\right)^{-0.403} C_t^{-1/79}\beta^{0.744}$ D_h=14.92 mm	1.223 m/s	10.4%

Table 5. Velocity Variation between the Peak Velocity and Central Core Velocity at Various Lateral Sections

x/D_p	V_{avg}	V_{core}	Variation
0.53	(1.3+1.26)/2=1.28 m/s	0.56 m/s	56%
0.79	(1.31+1.27)/2=1.29 m/s	0.42 m/s	67%
1.05	(1.2+1.17)/2=1.185 m/s	0.49 m/s	59%
1.32	(1.19+1.09)/2=1.14 m/s	0.51 m/s	55%
1.58	(1.04+1.01)/2=1.025 m/s	0.48 m/s	53%
1.84	(0.93+0.91)/2=0.92 m/s	0.5 m/s	46%
2.11	(0.94+0.94)/2=0.94 m/s	0.64 m/s	32%
2.37	(0.85+0.79)/2=0.82 m/s	0.56 m/s	32%
2.63	(0.83+0.8)/2=0.815 m/s	0.57 m/s	30%
2.89	(0.71+0.63)/2=0.67 m/s	0.6 m/s	10%
3.16	(0.72+0.62)/2=0.67 m/s	0.61 m/s	9%
3.42	(0.63+0.69)/2=0.66 m/s	0.66 m/s	0%
3.68	0.57 m/s	0.57 m/s	(end of zone)

Table 6. Comparison of the Suggested Length of Zone of Flow Establishment by Previous Researchers

Source	Length of zone	Acquisition method
Current measurement	x/D_p=3.68	Measurement
Albertson *et al.* (1950)	x/D_{or}=6.20	Prediction
Blaauw & van de Kaa (1978)	x/D_p=2.18	Measurement
Fuehrer *et al.* (1981)	x/D_p=2.60	Measurement
Verhey (1983)	x/D_p=2.77	Measurement
Hamill (1987)	x/D_p=2.00	Measurement
Stewart (1992)	x/D_p=3.25	Measurement

Albertson *et al*. (1950) suggested the length of this zone is x/D_{or}=6.2. However, the length defined by Albertson *et al*. (1950) is flawed as the plain water jet used has no rotational component of velocity, and is less diffusive than a rotating propeller jet. Measurements found by earlier researchers predict shorter lengths of zone of flow establishment and are given in Table 6.

3.1.4 Position of Maximum Velocity from the Rotation Axis within the Zone of Flow Establishment

Oebius and Schuster (1975) suggested the radial position of the maximum velocity drops rapidly (about 70%) from x/D_p=0 (efflux plane) to x/D_p=0.26 downstream (Fig. 10). Current investigation found that the radial position of maximum axial velocity is constant along the zone of flow establishment from x/D_p=0 (efflux plane), except a rogue point was found at x/D_p=0.79 downstream. All the other 13 radial positions of maximum axial velocity at various lateral sections occur at the same position. The measurements show the positions of the maximum velocity from the rotation axis within the zone of flow establishment remains as a constant location of r/R_p=0.53 from rotation axis.

Table 7 shows two proposals of the maximum velocity position along the rotation axis. Current measurements show the maximum velocity position is constant along the rotation axis. The constant maximum velocity position may be due to the entrainment was occurred inwardly and outwardly with the reduction of velocity magnitude. The maximum velocity position is balanced by the entrainment from both the directions. The drop of maximum velocity position from Oebius and Schuster (1975) may be due to the unbalance inward and outward entrainments and therefore the position was switched to the central core.

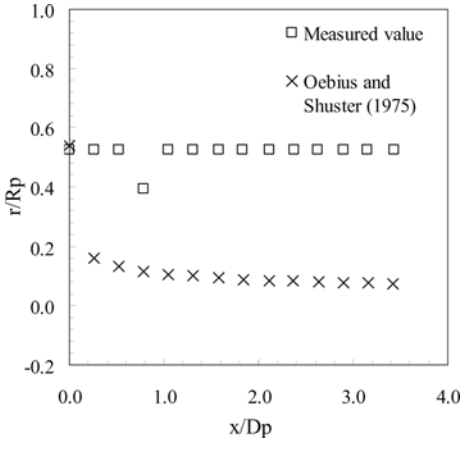

Fig. 10. Position of the Maximum Velocity (r/R_p, R_p=propeller radius) from the Rotation Axis versus Longitudinal Distance (x/D_p, D_p=propeller diameter) within Zone of Flow Establishment

Table 7. Comparison between the Measured Position of the Peak of Axial Velocity within the Zone of Flow Establishment and Previous Research

Source	Equation	Comparison
Oebius and Shuster's (1975)	$R_m = 0.3R_{mo}\left(\frac{X}{R_{mo}}\right)^{-0.3}$ where $R_{mo} = 0.67(R_p - R_h)$, R_p=0.076 m and R_h=0.01492 m	non-linear distribution
Measured value	r/R_p=0.53	constant

3.1.5 Extent of the Zone of Flow Establishment

The distribution of the axial component of velocity was presented using the lateral sections taken at the x/D_p=0, x/D_p=1.57, x/D_p=2.37 and x/D_p=3.68, as shown in Fig. 11. The current measurements were compared with the semi-empirical equations of Albertson *et al*. (1950) and Hamill (1987) (Table 8). The axial velocity used in this section is the average velocity of the two axisymetrical sides within a diffusing propeller jet.

Hamill (1987) reported the distribution of the axial component of velocity was found to increase from the low velocity core at the rotation axis, along the blade to a peak velocity value and then decrease rapidly to the tip of the blade, at the initial efflux

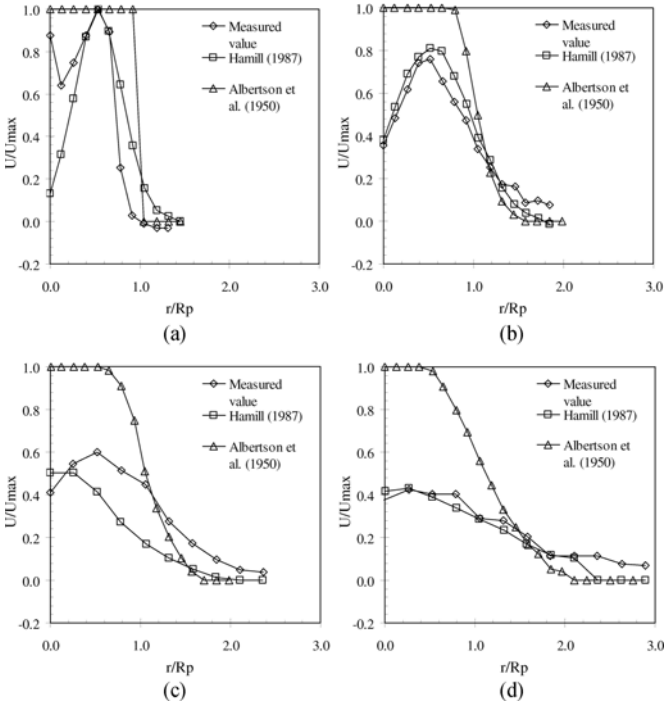

Fig. 11. Comparison of the Dimensionless Axial Velocity Distribution between the Current Measurements and the Earlier Researches: (a) x/D_p=0, (b) x/D_p=1.57, (c) x/D_p=2.37, (d) x/D_p=3.68

Table 8. Comparison of Axial Velocity Distribution between the Current Experimental Measurements and Existing Semi-empirical Equations

Source	Equation	Comparison
Albertson *et al.* (1950)	$0 \le x/D_{or} < 6.2$ (zone of flow establishment) $\frac{V_{x,r}}{V_o} = e^{\left[\left(r+Cx-\frac{D_{or}}{2}\right)^2/(2(Cx)^2)\right]}$ $x_o/D_{or} = 1/(2C)$ used to determine length of potential core at local section, C= 0.081 x_o=6.2D_{or} $V_0 = 1.59nD_p\sqrt{C_t}$ (1.274 m/s)	Albertson's (1950) plain jet is the foundation for the propeller jet investigation. However, a propeller jet shows no constant maximum velocity (potential core) within the zone of flow establishment.
Hamill (1987)	$R_{mo} = 0.67(R_p - R_h)$ $V_o = 1.33nD_p\sqrt{C_t}$ x/D_p=0 - x/D_p=0.5 $\frac{V_{x,r}}{V_{\max}} = e^{\left[-\frac{1}{2}\left((r-R_{mo})/\left(\frac{R_{mo}}{2}\right)\right)^2\right]}$ x/D_p=0 - x/D_p=2 $\frac{V_{x,r}}{V_{\max}} = e^{\left[-\frac{1}{2}\left((r-R_{mo})/\left(\frac{R_{mo}}{2}+0.075(X-R_p)\right)\right)^2\right]}$ x/D_p>2.0 $\frac{V_{x,r}}{V_{\max}} = e^{\left[-22.2\left(\frac{r}{X}\right)^2\right]}$	Hamill (1987) included the low velocity core along the rotation axis within the zone of flow establishment into the equations

plane and throughout the zone of flow establishment. The low velocity core found at the rotation axis within the zone of flow establishment is due to the influence of the propeller hub. The flow pattern reported by Hamill (1987) has been widely accepted by other researchers such as Stewart (1992) and McGarvey (1996). Current experimental measurement shows the similar flow pattern as reported by Hamill (1987) (Fig. 11a).

The profile of the axial velocity is due to the geometry of a ship's propeller. The hub of a propeller produces no forward thrust to the propeller and therefore a low velocity core occurs at the rotation axis. However, there is an additional disturbance of the hub which may cause an increase of velocity at the region very close to the hub. This increase of velocity close to the hub would vanish very fast at certain distance downstream. Hamill (1987) suggested the thrust produced by a propeller is normally governed by the pitch and the blade area ratio. The blade section close to the hub is small and this blade section increases with radial distance to a maximum value. The axial velocity close to the hub therefore increases radially to a velocity peak, depending on the width of blade section. The blade section then decreases to zero at the tip, and therefore the velocity decreases from the velocity peak down to zero at the tip (Fig. 11b-d).

Albertson *et al*. (1950) reported the velocity distribution at any section within a submerged jet to follow the general trend of a Gaussian normal distribution. The current experimental results agreed with the Gaussian normal distribution suggested by Albertson *et al*. (1950). However, current experimental result did not agree with the constant maximum velocity core at the zone of flow establishment suggested by Albertson *et al*. (1950). Albertson *et al*. (1950)'s velocity profile is incorrect compared to the current experimental measurement. The experimental measurements agreed with the refined equations proposed by Hamill (1987).

The velocity differences between the current measurements and Albertson *et al*. (1950) are mainly due to the method of producing a jet. Albertson *et al*. (1950) produced a plain water jet from an orifice and therefore a flat velocity profile was found at the central axis, as showed in Fig. 11(a). For comparison between the current measurements and Hamill (1987)'s results, Hamill (1987) used a pitot tube to acquire the velocity measurement and therefore the hub vortex at the rotation axis was not captured, as showed in Fig. 11(a). The differences of velocity distribution between the current measurements and Hamill (1987)'s results at further downstream was due to the use of two different propellers.

3.2 Tangential Component of Velocity

Brewster (1997) reported that the tangential component of velocity was the second largest contributor to the resultant velocity field of the propeller wash. Prosser (1986) estimated the magnitude of the maximum tangential velocity was approximately 30% of the maximum axial velocity.

The current experimental measurements confirmed that the tangential component of velocity was the second largest contributor to the resultant velocity field. However, the average of the maximum tangential velocities of the two axisymetrical sides (1.23 m/s and 1.00 m/s) is 1.12 m/s, whereas the average of the maximum axial velocities of two axisymetrical sides (1.39 m/s and 1.34 m/s) is 1.365 m/s. The maximum tangential component of velocity is therefore 82% of the maximum axial velocity, which contradicts the 30% approximation by Prosser (1986). Prosser (1986) may underestimate the magnitude of tangential velocity due to the limitation of the measurement system used at that time.

The influence of the tangential velocity after 280 mm (x/D_p=3.68) is less significant, with the magnitude of the tangential velocity being lower than 0.1 m/s (9% of the average of the maximum tangential velocities 1.12 m/s).

3.2.1 Extent of the Tangential Component of Velocity

Petersson *et al*. (1996) and Brewster (1997) reported the tangential velocity profile to have two peaks. The first peak corresponds to the point at which the hub and the propeller blades were joined and the second peak was present at a point near to the tip of the propeller.

However, Petersson *et al*. (1996) believed the first peak was located at radial distance r/R_p=0.15 from the rotation axis, the second peak located at r/R_p=0.65, and decreased simultaneously along the longitudinal axis to merge at x/D_p=1.5 downstream. Brewster (1997) believed these two peak velocities to occur at radial distance r/R_p=0.3 and r/R_p=0.8 at the initial efflux plane, and merge into one peak velocity at x/D_p=0.8 downstream along the longitudinal axis and the one peak velocity located at approximately radial distance r/R_p=0.5.

The experimental measurements show the two peak velocities to occurs at radial distance r/R_p=0.13 and r/R_p=0.66 and merge into one peak velocity at x/D_p=1.05 downstream (Fig. 12). The

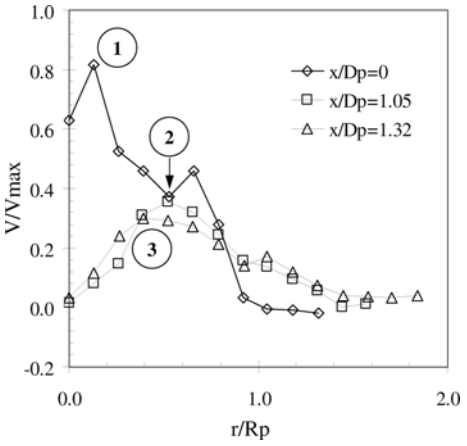

Fig. 12. Tangential Velocity Distribution within a Diffusing Propeller Jet, from Initial Efflux Plane (x/D_p=0) up to x/D_p=1.32 Downstream (Where, (1) The region close to propeller has two velocity peaks (r/R_p=0.14 and r/R_p=0.66) occurs up to x/D_p=1.05 downstream; (2) From x/D_p=1.05 downstream, two velocity peaks combine into one peak at radial position r/R_p=0.52; (3) From x/D_p=1.32 downstream, velocity peak moves closer to the rotation axis and the tangential velocity pattern remains constant further downstream.)

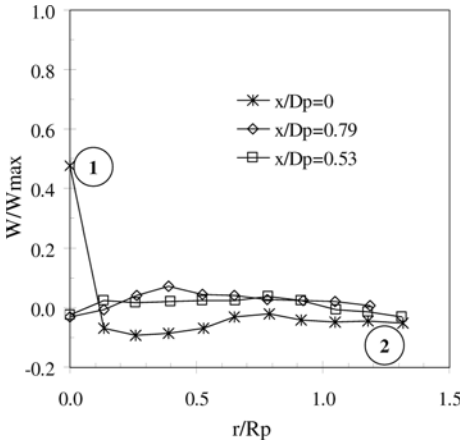

Fig. 13. Radial Velocity Distribution within a Diffusing Propeller Jet (Where, (1) Negative radial velocity close to the rotation axis shows the water penetration into central core; (2) Negative radial velocity at the end of each lateral section, shows ambient water being entrained into jet, from efflux plane (x/D_p=0).)

measured position of first velocity peak close to the hub has a 15% variation compared to the position reported by Petersson *et al*. (1996). The variation between the measured position and the position reported by Brewster (1997) for the first velocity peak close to the hub is 131%, which the variation is higher than that reported by Petersson *et al*. (1996). The variation of the second velocity peak close to the tip between the measured position and that reported by Petersson *et al*. (1996) is only 2% and the variation of the second velocity peak between the measured position and Brewster (1997)'s position is 21%.

From x/D_p=1.05 behind the propeller, the two velocity peaks combine into one peak at radial distance r/R_p=0.52. The one velocity peak pattern is established by x/D_p=1.05. However, the location of this velocity peak moves closer to the rotation axis. The location of this velocity peak remains constant from x/D_p=1.32 downstream with a radial position r/R_p=0.4 for the rest of the diffusing jet.

3.3 Radial Component of Velocity

McGarvey (1996) reported the magnitude of radial component of velocity was approximately 30% of the axial velocity along the face of the propeller. Current measurement shows the radial velocity of the two axisymetrical sides are 0.13 m/s and 0.24 m/s. The average radial velocity is 0.19 m/s, which is 14% of the axial velocity (1.365 m/s for this case). At 14% of the axial velocity, the measured radial velocity is lower than the 30% of axial velocity suggested by McGarvey (1996).

The measurement shows that the extreme velocity 0.65 m/s (53% of the efflux velocity) was recorded close to the propeller hub at the efflux plane. However, this extreme velocity was treated as an additional disturbance rather than a maximum velocity at efflux plane. Apart from the extreme radial velocity due to the hub, the velocity remains low along the longitudinal section (maximum radial velocity is only 14% of the efflux velocity). The low velocity magnitude along the longitudinal section can be seen measurements.

3.3.1 Extent of the Radial Component of Velocity

McGarvey (1996) reported the radial component of velocity increased from the hub to a peak velocity and thereafter decrease towards the blade tip. Brewster (1997) reported a portion of flow was directed towards the rotation axis to penetrate the low velocity core.

Current measurements found the radial velocity increases from the hub to a peak velocity and thereafter decrease towards the blade tip (Fig. 13), as reported by McGarvey (1996). In addition, the measurements show the flow close to the rotation axis penetrates into low velocity core and the flow at the jet boundary entrained the ambient still water into the jet, as reported by Brewster (1997).

3.4 Turbulence Fluctuations from Dantec LDA System

Figure 14 shows the overview of the absolute values of x-component (U), y-component (V) and z-component (W) of velocity and their fluctuations (u'), (v') and (w') from the Dantec LDA system, at efflux plane (x/D_p=0). The axial, tangential and radial fluctuations are in the same order of magnitude. The axial, tangential and radial turbulence intensities show a surge at the rotation axis (radial location r/R_p=0). A smaller surge of turbulence intensity also occurs at radial distance r/R_p=0.8 and r/R_p=-0.8 on both sides close to the jet boundary (where ambient still water is being entrained into the jet).

As reported in the mean velocity investigation (Stewart, 1992), the fluid mixing occurs inwardly to penetrate the low velocity core at the jet centre and outwardly to entrain the ambient still

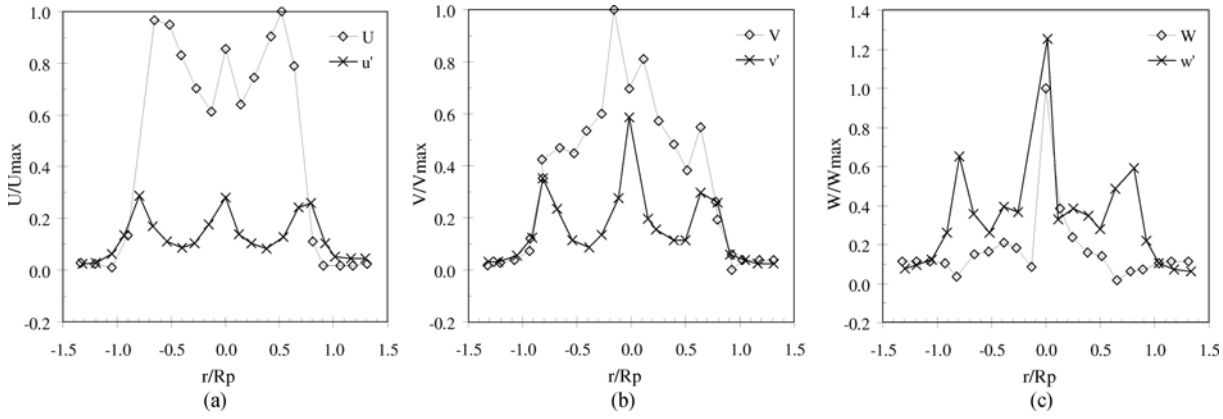

Fig. 14. Dimensionless Time-averaged Velocity and Turbulent Fluctuation: (a) Axial Component, (b) Tangential Component, (c) Radial Component

water into the jet. The high turbulence intensity occurring at the central core and at the regions close to the jet boundary may be due to the fluid mixing. The higher turbulence intensity occurs at the central core rather than the jet boundary, which may due to the combination of fluid mixing and hub disturbance at the efflux plane ($x/D_p=0$).

4. Conclusions

The study of the time-averaged velocity within the zone of flow establishment from a ship's propeller using a Laser Doppler Anemometry (LDA) experimental approach has been demonstrated. By analysing the experimental measurements, the axial, tangential and radial components of velocity and turbulence intensity were investigated and the following conclusions can be drawn:

1. The demarcation of the zone of flow establishment was found at $3.68D_p$ downstream from the efflux plane, which was longer than the $3.25D_p$ proposed by Stewart (1992). Experimental measurements found that the axial component of velocity showed two peaked ridges at the zone of flow establishment and then combined into a peaked ridge in the zone of established flow.
2. The propeller jet in the zone of flow establishment was reasonably axisymetric about the rotation axis. From the efflux plane ($x/D_p=0$) up to $x/D_p=2.63$ downstream, the lateral sections showed strong axisymetrical peak velocity profiles at both sides about the rotation axis. Two-peaked profiles became less axisymetric and swayed to the left and right from $x/D_p=2.89$ to $x/D_p=3.42$ downstream. The variation between the velocity values of two sides about the rotation axis was up to 48% within the zone of flow establishment, occurred at $x/D_p=3.16$, based on the half-width analysis.
3. Current measurements showed that the position of the maximum axial velocity within the zone of flow establishment was at a constant radial position of $r/R_p=0.53$. Current measurements contradicted to Oebius and Schuster (1975)'s suggestion that the radial position of the maximum velocity dropped rapidly (about 70%) from $x/D_p=0$ (efflux plane) to $x/D_p=0.26$ downstream.
4. Experimental measurements found that the axial component of velocity was the main contributor to the velocity magnitude. The tangential component contributed to the rotation while the radial component which contributed to the diffusion, were the second and third contributors to the velocity magnitude within the propeller jet.
5. The absolute value of efflux velocity from the experimental measurements has variations of 6.7%, 21.9%, 9.9% and 10.4% respectively compared to the axial momentum theory and also those proposed by Hamill (1987), Stewart (1992) and Hashmi (1993).
6. The current experimental measurements showed that the tangential component of velocity was 82% of the maximum axial velocity, which contradicted the 30% approximation by Prosser (1986).
7. For the distribution of tangential velocity, measurements found two peak velocities to occurred at the efflux plane at radial distance of $r/R_p=0.13$ and $r/R_p=0.66$ and merged into one peak velocity at $x/D_p=1.05$ downstream, with the peak occurring at a radial distance of $r/R_p=0.52$. The location of this velocity peak moved closer to the rotation axis until a distance of $x/D_p=1.32$ downstream where it occurred at a radial position of $r/R_p=0.4$ and remained at this position for the rest of the jet.
8. The radial component of velocity showed that the extreme velocity 0.65 m/s (53% of the efflux velocity) was recorded close to the propeller hub at the efflux plane. Apart from the extreme radial velocity due to the hub, the velocity remained low along the longitudinal section (maximum radial velocity is only 14% of the efflux velocity).
9. For the distribution of radial velocity, measurements found the radial velocity increased from the hub to a peak velocity and thereafter decreased towards the blade tip, as reported by McGarvey (1996). In addition, negative radial velocity was also found close to the rotation axis, where the jet penetrated into low velocity core, as reported by Brewster (1997).

10. The axial, tangential and radial turbulence intensities showed a surge at the rotation axis (radial location $r/R_p=0$). A smaller surge of turbulence intensity also occured at radial distance $r/R_p=0.8$ and $r/R_p=-0.8$ on both sides close to the jet boundary (where ambient still water was being entrained into the jet).

Notations

C_t: Thrust coefficient of the propeller
D_h: Diameter of hub (m)
D_o: Diameter of orifice exit (m)
D_p: Propeller diameter (m)
E_o: Hashmi (1993)'s efflux velocity coefficient
L_m: Length term dependant on the number of blades
max: Maximum value
N: Number of blades
N_s: Number of samples
n: Speed of rotation of the propeller (rps)
P!: Propeller pitch ratio
R_p: Radius of propeller (m)
R_h: Radius of hub (m)
Re_{prop}: Reynolds number of the propeller
Re_{flow}: Reynolds number of the flow
R_{mo}: Location efflux velocity (m)
r: Radial distance from propeller centre (m)
U: Axial velocity (m/s)
u!: Axial turbulence fluctuation (m/s)
V: Tangential velocity (m/s)
V_o: Efflux velocity (m/s)
v!: Axial turbulence fluctuation (m/s)
W: Radial velocity (m/s)
w!: Radial turbulence fluctuation (m/s)
x: Longitudinal distance from propeller (m)
β: Blade area ratio
ν: Kinematic viscosity of the fluid
θ: Rake angle (degree)
ς: Stewart (1992)'s efflux velocity coefficient

Acknowledgements

The current research is supported by UM/MOHE High Impact Research (HIR) grant (account No. H-1600-00-D000047) from Malaysia government. The research was supported by the National Natural Science Foundation of China (grant no. 51006019/E060704) and SPUR studentship from Queen's University Belfast.

References

Albertson, M. L., Dai, Y. B., Jensen, R. A., and Rouse, H. (1950). "Diffusion of a submerged jets." Transcript of the ASCE, Vol. 115, No. 409, pp. 639-669.

Berger, W., Felkel, K., Hager, M., Oebius, H., and Schale, E. (1981). "Courant provoque par les bateaux protection des berges et solution pour eviter l'erosion du lit du haut rhin." *P.I.A.N.C., 25th Congress*, Section I-1, Endinburgh.

Bergh, H. and Cederwall, K. (1981) *Propeller erosion in harbours*, Bulletin No TRITA-VBI-107, Hydraulics Laboratory, Royal Institute of Technology, Stockholm, Sweden.

Blaauw, H. G. and van de Kaa, E. J. (1978). *Erosion of bottom and sloping banks caused by the screw race of manoeuvring ships*, Publication No 202, July 1978, Delft Hydraulics Laboratory, Netherlands.

Brewster, P. M. (1997). *Modelling the wash from a ship's propeller*, PhD Thesis, Queen's University of Belfast, UK.

Carlton, J. S. (1994). *Marine propellers and propulsion*, Butterworth Heinemann, London.

Dantec (2003). *BSA flow software version 2.1 user's guide and installation*, Dantec Dynamics, Skovlunde

Dargahi, B. (2003). "Three-dimensional modelling of ship-induced flow and erosion." *Proceeding of the Institution of Civil Engineers: Water & Maritime Engineering*, Issue WM2, pp. 193-204.

EN-ISO-3715-1 (2004). *Ships and marine technology, propulsion plants for ships, part 1: Vocabulary for geometry of propellers*, Tech. Rep., European Committee for Standardisation

Fuehrer, M. and Rmisch, K. (1977). "Effects of modern ship traffic on islands and ocean waterways and their structures." *P.I.A.N.C. 24th Congress*, Leningrad, Vol. Sections 1-3.

Fuehrer, M. and Rmisch, K. (1987). "Propeller jet erosion and stability criteria for bottom protection of various constructions." *P.I.A.N.C.*, Vol Bulletin No. 58.

Gaythwaite, J. (2004). *Design of marine facilities for the berthing, mooring, and repair of vessels*, ASCE Publications.

Gerr, D. (2001) *Propeller handbook*, The Complete Reference for Choosing, Installing and Understanding Boat Propellers, International Marine, Camden.

Hamill, G. A. (1987). *Characteristics of the screw wash of a manoeuvring ship and the resulting bed scour*, PhD Thesis, Queen's University of Belfast, UK.

Hamill, G. A., McGarvey, J. A., and Hughes, D. A. B. (2004). "Determination of the efflux velocity from a ship's propeller." *Proceedings of the Institution of Civil Engineers: Maritime Engineering*, Vol. 157, No. 2, pp. 83-91.

Hamill, G. A., Ryan, D., and Johnston, H. T. (2009). "Effect of rudder angle on propeller wash velocities at a seabed." *Proceedings of the Institution of Civil Engineers: Maritime Engineering*, Vol. 162, pp. 27-38.

Hashmi, H. N. (1993). *Erosion of a granular bed at a quay wall by a ship's screw wash*, PhD Thesis, Queen's University of Belfast, UK.

Kang, S. W., Oh, B. C., Park, K. S., and You, S. H. (1999). "Near-field dilution of wastewater effluents discharged from submerged ocean outfalls in masan bay." *KSCE Journal of Civil Engineering*, Vol. 3, No. 4, pp. 395-405.

Kim, D. G. and Seo, I. W. (2004). "Numerical simulations of the buoyant flow of heated water discharged from submerged side outfalls in shallow and deep water." *KSCE Journal of Civil Engineering*, Vol. 8, No. 2, pp. 255-263.

Kwon, S. J. and Seo, I. W. (2005). "Experimental investigation of wastewater discharges from a rosette type riser using piv." *KSCE Journal of Civil Engineering*, Vol. 9, No. 5, pp. 355-362.

Lam, W.-H., Hamill, G., Robinson, D., and Raghunathan, S. (2010). "Observations of the initial 3D flow from a ship s propeller." *Ocean Engineering*, Vol. 37, pp. 1380-1388.

Lam, W., Hamill, G. A., Robinson, D. J., and Raghunathan, S. (2012). "Semi-empirical methods for determining the efflux velocity from a

ship's propeller." *Applied Ocean Research*, Vol. 35, pp. 14-24.

Lam, W., Hamill, G. A., Song, Y. C., Robinson, D. J., and Raghunathan, S. (2011b). *Experimental investigation of the decay from a ship's propeller*, *China Ocean Eng.*, Vol. 25, pp. 265-284.

Lam, W., Hamil, G. A., Song, Y. C., Robinson, D. J., and Raghunathan, S. (2011c). "A review of the equations used to predict the velocity distribution within a ship s propeller jet." *Ocean Engineering*, Vol. 38, pp. 1-10.

Lam, W.-H., Song, Y., Raghunathan, S., Hamill, G., and Robinson, D. (2011a). "Investigation of a ship's propeller jet using momentum decay and energy decay." *Can. J. Civ. Eng*., Vol. 38, pp. 605-615.

McGarvey, J. A. (1996). *The influence of the rudder on the hydrodynamics and the resulting bed scour, of a ship's screw wash*, PhD Thesis, Queen's University of Belfast, UK.

Oebius, H. and Schuster. S. (1975). *Modelversuche zur frage der beschadigung von flussohlen durch die schiffahrt versuchsanstalt fur wasserbau und schiffbau*, Tech. Rep., Berlin, VWS-Bericht nr. 743/75.

Petersson, P., Larson, M., and Jonsson, L. (1996). "Measurements of the velocity field downstream of an impeller." *Journal of Fluids Engineering*, ASME, Vol. 118, No. 3, pp. 602-610.

Prosser, M. (1986). "Propeller induced scour." Tech. Rep., BHRA Project RP A01415, The Fluid Engineering Centre, Cranfield.

Qurrain, R. (1994). *Influence of the sea bed geometry and berth geometry on the hydrodynamics of the wash from a ship's propeller*, PhD Thesis, Queen's University of Belfast, UK.

Robakiewicz, W. (1987). "Bottom erosion as an effect of ship propeller action near the harbour quays." *PIANC*, Bulletin No. 58, pp. 89-106.

Ryan, D. (2002). *Methods for determining propeller wash induced scour in harbours*, PhD Thesis, Queen's University of Belfast, UK.

Seo, I. W. S., Kwon, S. J., and Yeo, H. K. (2004). "Merging characteristics of buoyant discharges from rosettetype diffusers in shallow water." *KSCE Journal of Civil Engineering*, Vol. 8, No. 6, pp. 679-688.

Stewart, D. P. J. (1992). *Characteristics of a ships screw wash and the influence of quay wall proximity*, PhD Thesis, Queen's University of Belfast, UK.

Sumer, B. M. and Fredsøe, J. (2002). *The mechanics of scour in the marine environment,* World Scientific.

Verhey, H. J. (1983) "The stability of bottom and banks subjected to velocities in the propeller jet behind ships." *8th International Harbour Congness*, Antwerp, Belgium

Delft Publication No303, April 1983, Delft Hydraulics Laboratory, Netherlands

van Blaaderen, E. A. (2006). *Modelling bow-thrusters induced flow near a quay wall*, Master's Thesis, Delft University of Technology, Netherland.

Whitehouse, R. (1998). *Scour at marine structures: A manual for practical applications*, Thomas Telfordr.

Yeh, P. H., Chang, K. A., Henriksen, J., Edge, B., Chang, P., Silver, A., and Vargas, A. (2009). "Large-scale laboratory experiment on erosion of sand beds by moving circular vertical jets." *Ocean Engineering*, Vol. 36, pp. 248-255.

Yülsel, A., Celikoglu, Y., Cevik, E., and Yüksel, Y. (2005). "Jet scour around vertical piles and pile groups." *Ocean Engineering*, Vol. 32, pp. 349-362.